THE ASTRONOMICAL JOURNAL, 116:657–672, 1998 August

HUBBLE SPACE TELESCOPE WIDE FIELD PLANETARY CAMERA 2 IMAGING OF UGC 12695: A REMARKABLY UNEVOLVED GALAXY AT LOW REDSHIFT

KAREN O'NEIL AND G. D. BOTHUN
Department of Physics, University of Oregon, Eugene, OR 97403; karen@moo.uoregon.edu, nuts@moo2.uoregon.edu
C. D. IMPEY
Department of Astronomy and Steward Observatory, 933 North Cherry Avenue, University of Arizona, Tucson, AZ 85721; impey@as.arizona.edu
AND
S. MCGAUGH
Department of Physics, Rutgers University, P.O. Box 849, Piscataway, NJ 08854; mcgaugh@physics.rutgers.edu
Received 1998 February 17; revised 1998 May 7

ABSTRACT

Utilizing the F814W and F300W filters, short-exposure *Hubble Space Telescope* Wide Field Planetary Camera 2 images were taken of UGC 12695, a nearby ($z \sim 0.021$) low surface brightness disk galaxy. UGC 12695 has an unusual morphology, consisting of a Y-shaped nucleus surrounded by a faint spiral arm with a number of bright H II regions interspersed throughout the galaxy. Surface photometry indicates that the majority of recent star formation in this galaxy occurred in these very localized regions, most of which have a radius of $\lesssim 2''$. This uneven stellar distribution, combined with the galaxy's overall extremely blue color and low metallicity, indicates that UGC 12695 is an unevolved galaxy. Some of the structural peculiarities of this galaxy arise because a number of background galaxies, previously thought to be morphological components of this galaxy, are showing through both the outer nucleus and spiral arms of UGC 12695. Surface photometry of these galaxies shows them to be fairly small ($\alpha < 1''.8$) disk galaxies with total magnitudes ranging from 19.6 through 24.2 mag and central surface brightnesses in the range 20.2 mag arcsec$^{-2} \leq \mu(0) \leq$ 23.1 mag arcsec^{-2}. When possible, the U, B, V, and I colors of these galaxies were measured using ground-based images, which show the galaxies to be fairly red, indicating that they are likely at redshifts $z \geq 0.5$. Inclusion of them in the photometry of UGC 12695 makes the galaxy appear significantly redder. When these galaxies are masked out, the resultant $U-I$ color of UGC 12695 is -0.2 ± 0.1, making it perhaps the bluest galaxy ever measured in this color system and confirming its nature as a very unevolved galaxy at low redshift. Spectroscopy of these background galaxies, through the transparent disk of UGC 12695, may help to clarify its chemical evolution and current heavy-element content.

Key words: galaxies: evolution — galaxies: fundamental parameters — galaxies: individual (UGC 12695) — galaxies: ISM — galaxies: photometry — Magellanic Clouds

1. INTRODUCTION

Studies of low surface brightness (LSB) galaxies have revealed a population of relatively unevolved systems compared with the traditional Hubble sequence of spirals (Bothun, Impey, & McGaugh 1997). Although the overall properties of LSB galaxies span a wide range in color, gas content, and metallicity (see O'Neil et al. 1997; McGaugh & de Blok 1997), there is a significant subset that have extremely blue colors, high gas contents, and low metallicities. These are obvious candidates for being the most unevolved systems in the nearby universe. Among these kinds of systems, UGC 12695 may be the best example of a very unevolved and quite young LSB galaxy.

Previous studies of UGC 12695 have shown it to have a very blue color, low metallicity, high gas mass fraction, and unique morphological structure (McGaugh & de Blok 1997; McGaugh, Schombert, & Bothun 1995; McGaugh 1994; McGaugh & Bothun 1994; Klein et al. 1992; Schneider et al. 1990; Bottinelli et al. 1990; Lewis 1987). This galaxy is relatively isolated, with its nearest neighbor (UGC 12687) residing 11'.2 ($\sim$10 galaxy diameters) away. Because of its intriguing properties, UGC 12695 was a high-priority target in our *Hubble Space Telescope* (*HST*) Wide Field Planetary Camera 2 (WFPC2) survey of selected LSB galaxies to further study their structure and evolution. In this paper, we report on the remarkable nature of this galaxy as revealed by these new observations. Section 2 describes the observations and data reduction techniques. Section 3 describes the global properties of UGC 12695, while § 4 discusses some of the individual star-forming regions of the galaxy. In § 5, we discuss the background galaxies discovered within the WFPC2 images, and finally, in § 6 we consider the implications of our discoveries.

2. OBSERVATIONS AND DATA REDUCTION

Eight *HST* WFPC2 images were taken of UGC 12695 on 1997 January 7 using all four WFPC2 cameras. The nucleus of UGC 12695 was positioned in the WF3 field. Initial image processing occurred using the STSDAS pipeline, followed by additional reduction to eliminate cosmic rays and then to combine the images.

The WFPC2 consists of three wide-field (WF) cameras and one planetary camera (PC). The WF cameras have a focal ratio of f/12.9 and a field of view of $80'' \times 80''$ with each pixel subtending $0''.0996$. The three cameras form an L shape, with the PC completing the square. The PC has a focal ratio of f/28.3, a scale of $0''.0455$ pixel^{-1}, and an overall field of view of $36'' \times 36''$. Each camera has an 800×800

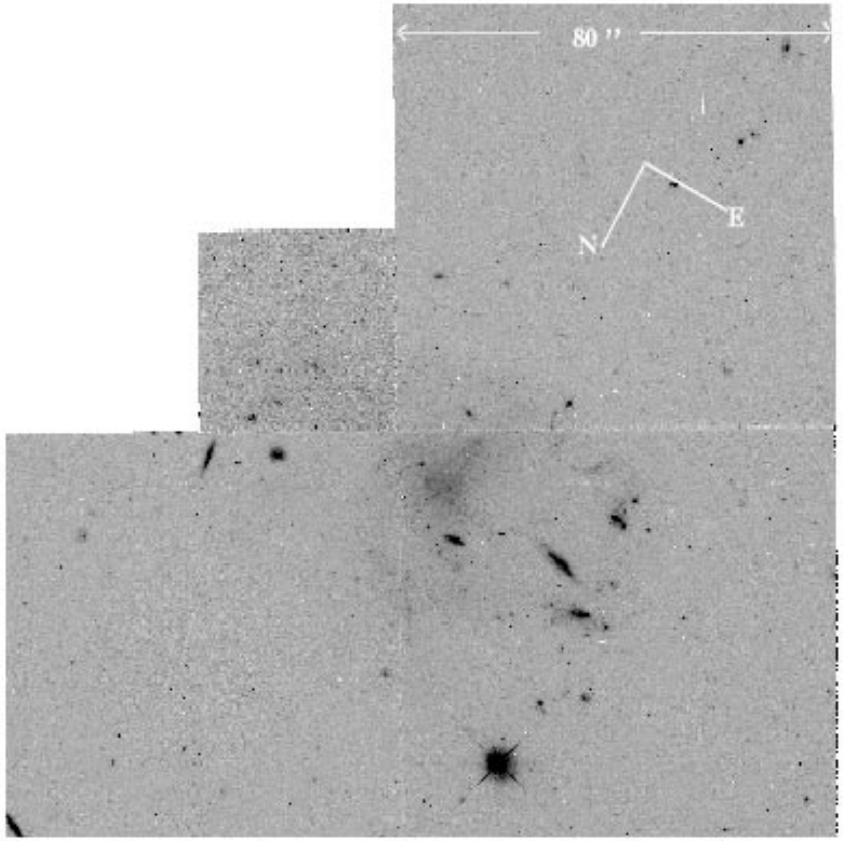

FIG. 1*a*

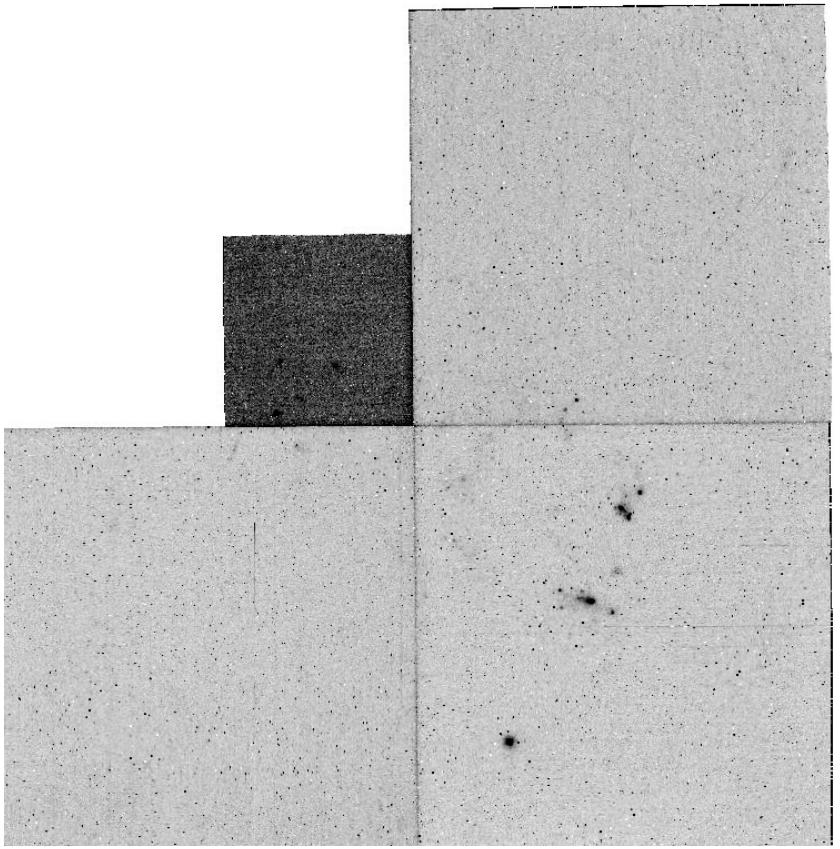

FIG. 1*b*

FIG. 1.—*HST* WFPC2 image of UGC 12695 taken through (*a*) the 814 (*I* band) filter and (*b*) the 300 (*U* band) filter with a 2000 s exposure time

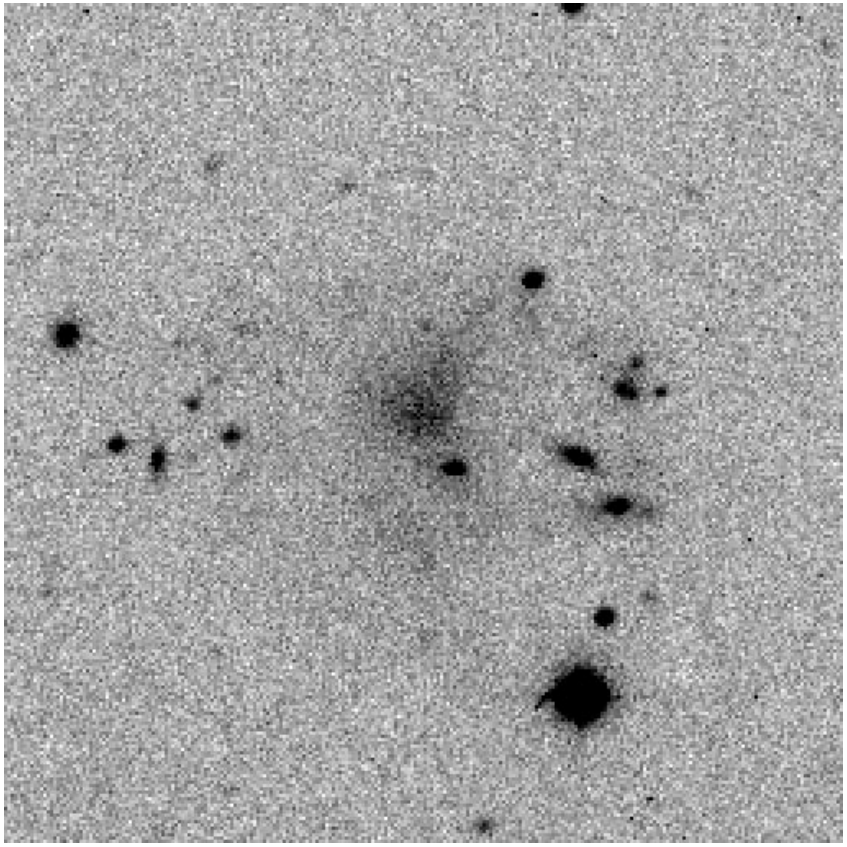

FIG. 2*a*

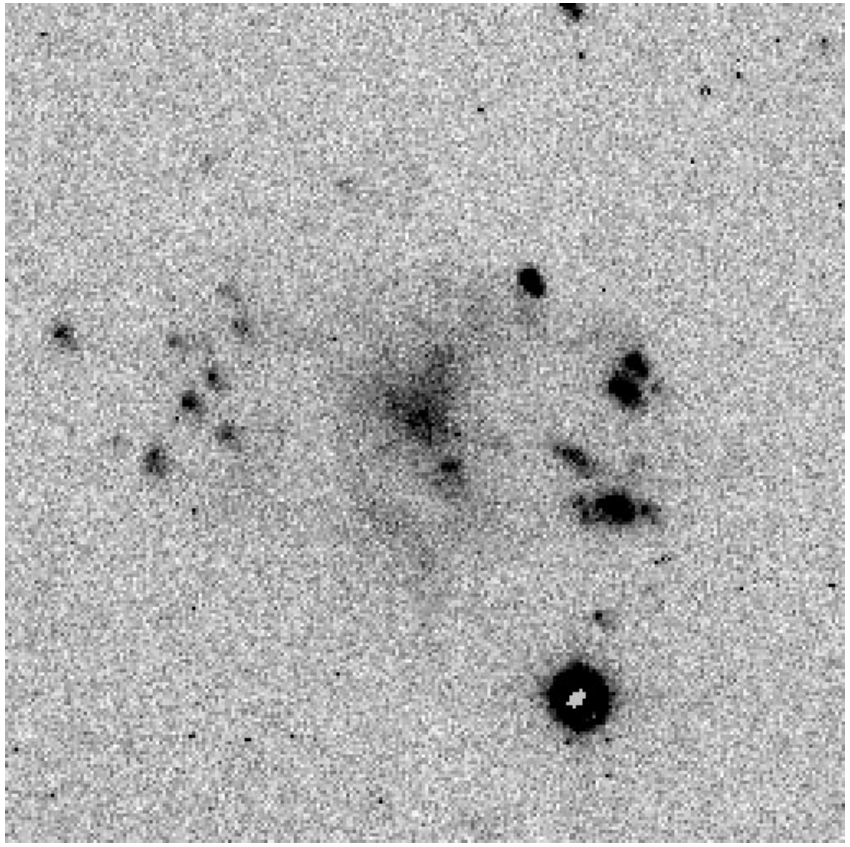

FIG. 2*b*

FIG. 2.—Images of UGC 12695 taken using the MDM 1.3 m telescope through the (*a*–*e*) *I*, *V*, *B*, *U* and continuum-subtracted Hα bands, respectively. The images are 124″ across, with north up and east to the left. In (*e*), the regions of Hα emission studied in § 4 are also labeled. See McGaugh (1992) for details on these images.

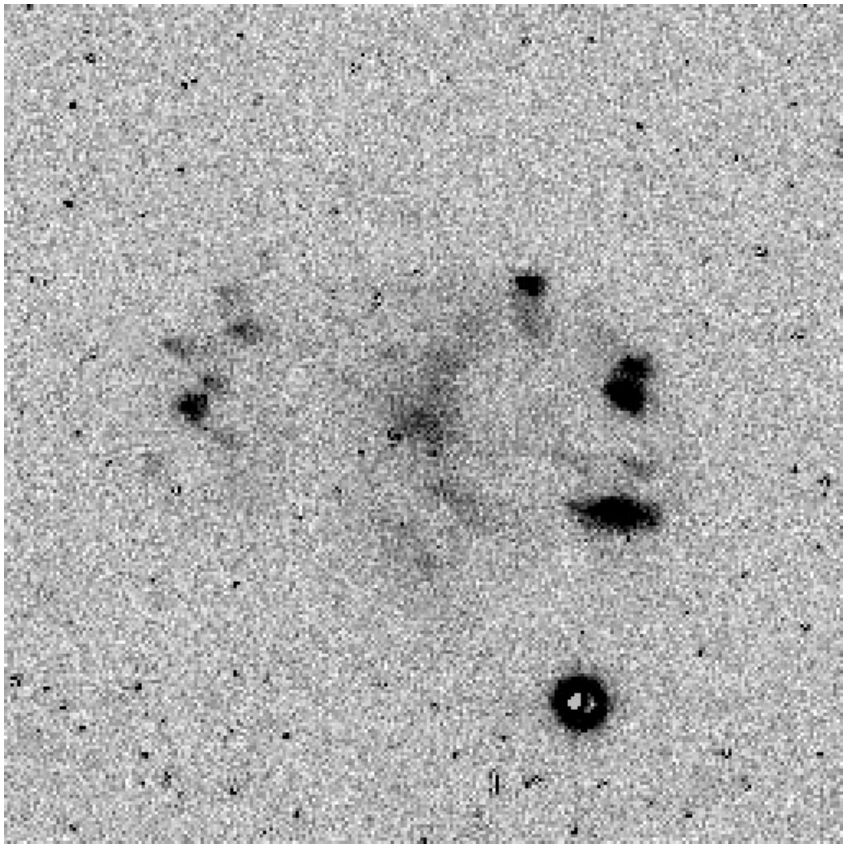

FIG. 2*c*

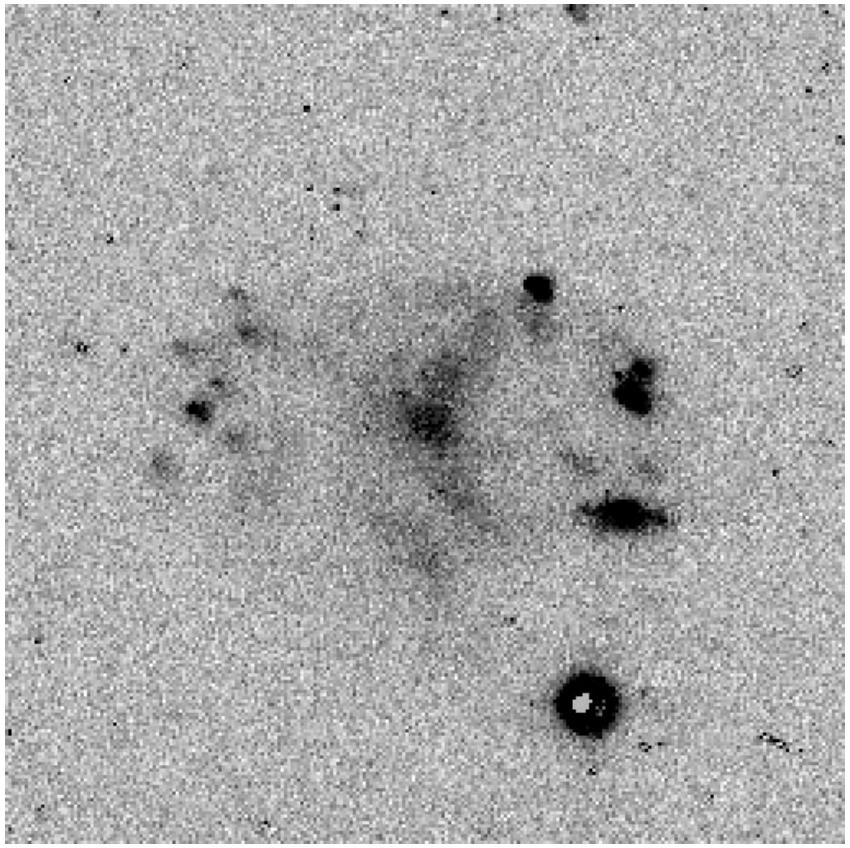

FIG. 2*d*

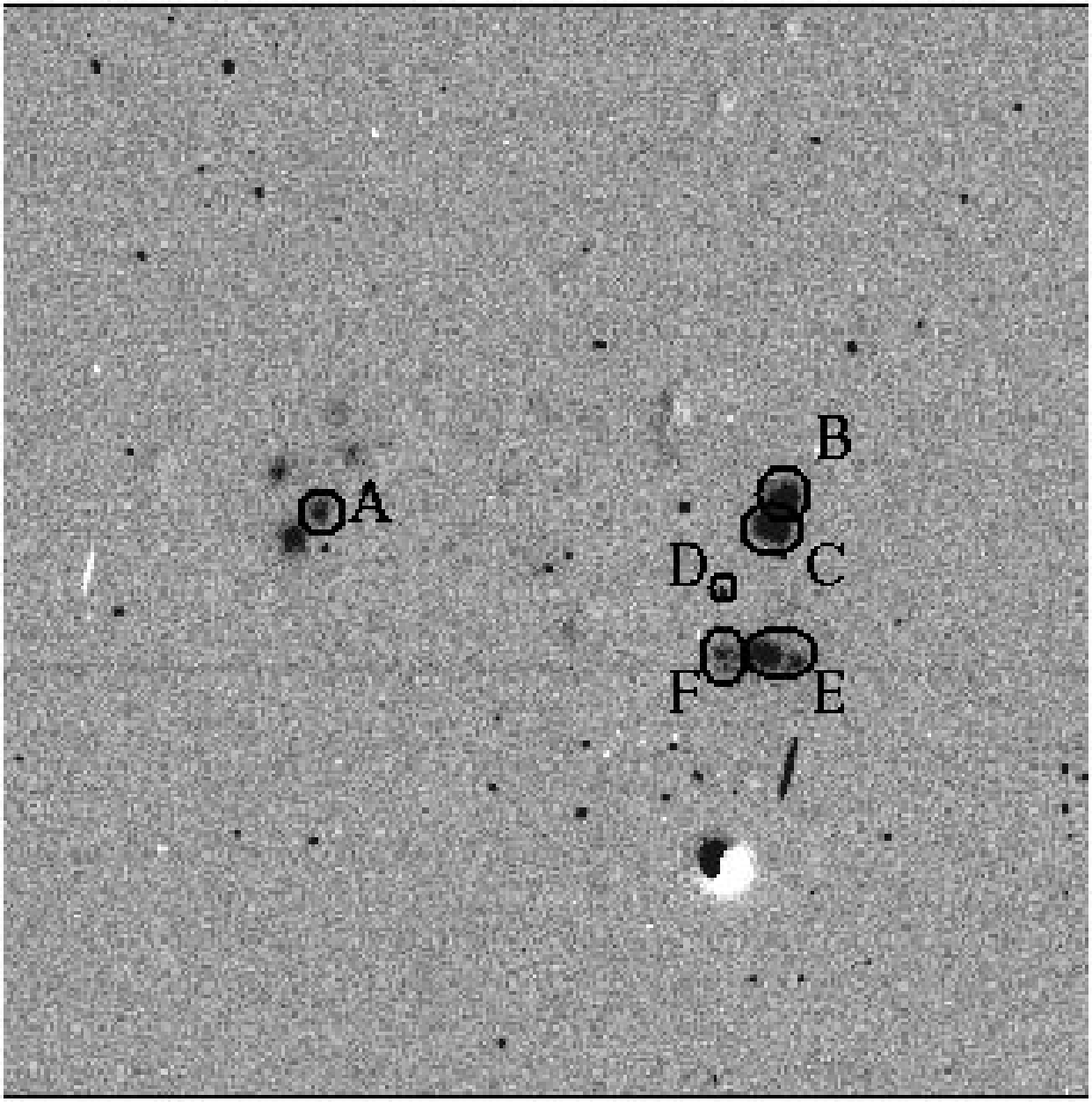

FIG. 2*e*

pixel silicon CCD with a thermoelectric cooler to suppress dark current. The WFPC2 has two readout formats—single-pixel resolution (FULL mode) and 2×2 pixel binning (AREA mode). All images taken through the F814W (hereafter 814) filter were taken in FULL mode while all images taken through the F300W (hereafter 300) filter were taken in AREA mode.

Images of UGC 12695 were taken through both the 814 and the 300 filters. The 814 filter is a broadband filter with $\lambda_0 = 7924$ Å and $\Delta\lambda_{1/2} = 1497$ Å. It is designed to be similar to the Johnson *I*-band filter. The 300 filter has $\lambda_0 = 2941$ Å and $\Delta\lambda_{1/2} = 757$ Å and is designed to be similar to the Johnson *U*-band filter. All images had 500 s exposure times. As the sensitivity level through the 814 filter images was considerably higher than through the 300 filter images (because of the CCD response) and UGC 12695 tended to be much brighter through the 814 filter, all galaxy identification and analysis were done with the 814 images. When possible, photometry for a galaxy was also done through the 300 filter.

Sky flat fields of the sunlit Earth were taken through each filter and routinely calibrated against an internal flat-field calibration system. The internal system consists of two lamps (optical and UV) illuminating a diffuser plate. The internal flats are used to monitor and correct for changes in the flat fields. Dark frames are averages of 10 calibration images taken over the space of 2 weeks. The intrinsic dark rate of the WFPC2 CCDs is $\lesssim 0.01\ e^-\ \text{pixel}^{-1}\ \text{s}^{-1}$. The calibration dark fields were scaled to the exposure time of each image. A bias field was generated for each image using extended-register pixels that do not view the sky.

The data reduction process was as follows: First, all known bad pixels were removed, using the static mask reference file. The bias level, calculated as described above, was

TABLE 1

GLOBAL PROPERTIES OF UGC 12695

Parameter	Value
(1) R.A. (J2000.0)	23 36 02.0
(2) Decl. (J2000.0).....	12 52 32
(3) V (km s^{-1})	6182
(4) d (Mpc)	4590
(5) $M_{\rm H\,I}$	9.62
(6) $M_{\rm dyn}$.....	9.98
(7) $M_{\rm H\,I}/L_B$	1.28
(8) f_g^B.....	0.62
(9) h (kpc)	8.4
(10) M_B	−18.92
(11) $\mu_B(0)$.....	23.8
(12) m_B	15.53
(13) $B-V$	0.26
(14) $U-B$	−0.11
(15) $V-I$	0.95

NOTE.—Units of right ascension are hours, minutes, and seconds, and units of declination are degrees, arcminutes, and arcseconds.

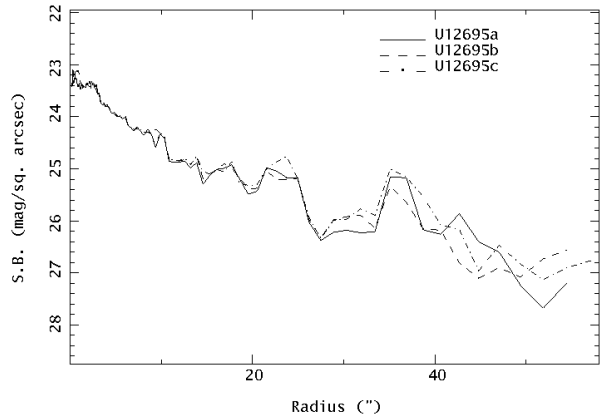

FIG. 3.—Surface brightness profile of UGC 12695 through the 814 filter. The solid line is the surface brightness profile with all background galaxies and Hα regions included in the analysis, the dashed line is UGC 12695 with all the background galaxies (except U2-74; see text) removed, and the dash-dotted line is UGC 12695 with both the background galaxies and all the Hα regions removed (see § 3). The errors in the surface brightness profiles are low, staying below 0.20 mag arcsec^{-2} up to a radius of 40″, after which the errors reach 0.30–0.50 mag arcsec^{-2} for the last three plotted points. This error comes primarily from uncertainties in the sky background. Our measured value is 21.6 counts pixel^{-1} with a mean error of 0.1 counts pixel^{-1}. This maps onto a mean surface brightness through the 814 filter of 21.5 mag arcsec^{-2} with a 1 σ isophotal detection at 27.4 mag arcsec^{-2} (e.g., 0.1 counts pixel^{-1}). Hence, we can do reliable isophotal detection down to 6 mag below sky with these data.

then removed from each frame. The bias image, generated to remove any position-dependent bias pattern, was then subtracted from the image, as was the dark-field image (described above). Flat-field multiplication was then performed using the fields described above. All the preceding image calibration was performed at the Space Telescope Science Institute (STScI) using the standard WFPC2-specific calibration algorithms (the pipeline).

Four images of 500 s each were taken through each filter. After the images were reduced, they were inspected for such obvious flaws as filter ghosts or reflections. Each frame was then shifted, registered, and combined, using the STSDAS CRREJ task to eliminate cosmic rays and other small-scale flaws ($\sigma = 10$, 8, and 6). The resultant images were checked by eye to ensure that any registration errors were under 0.5 pixels. The intensities were then reduced by a factor of 4 (using the IRAF IMARITH procedure) to yield the resultant image with mean intensity value from the four combined images. Finally, the images were mosaicked, using the STSDAS WMOSAIC task to create the complete WFPC2 image shown in Figure 1. The total flux was conserved in the mosaic step.

Background galaxy identification was done within the confines of the IRAF environment. Each image was enlarged by a factor of 4 and scanned by eye for nonstellar objects. By examining both processed images available for

TABLE 2

COLORS OF UGC 12695 DETERMINED FROM THE 814 AND 300 WFPC2 IMAGES

	INNER 2″			INNER 10″			INNER 30″		
METHOD	814	300−814	$U-I$	814	300−814	$U-I$	814	300−814	$U-I$
1	22.215	−0.541	2.159	19.426	−0.440	2.260	18.069	−2.750	−0.092
2	22.215	−0.541	2.159	19.509	−0.977	1.723	18.145	−2.879	−0.179
3	22.215	−0.541	2.159	19.511	−0.970	1.730	18.145	−2.883	−0.183

NOTES.—Row 1 lists the colors with both the background galaxies and all Hα regions included. Row 2 lists the results of masking the background galaxies. Row 3 lists the results of masking both the background galaxies and the Hα regions. All colors are within ±0.05.

TABLE 3

COLORS OF THE Hα REGIONS OF UGC 12695

Region	R.A. (J2000.0)	Decl. (J2000.0)	300−814	$U-I$	R[a] (arcsec)	300_T	814_T	$R_{\rm IT}$ (arcsec)
A	23 35 59.68	12 52 31.4	−2.167	0.533	0.63	21.194	22.511	1.09
B	23 26 04.21	12 52 25.5	−2.337	0.363	1.53	19.284	19.831	2.15
C	23 36 04.09	12 52 29.4	−2.627	0.077	2.62	17.964	19.941	3.31
D.....	23 36 04.25	12 52 39.9	−2.607	0.093	1.12	20.374	22.981	1.12
E	23 36 03.98	12 52 46.5	−2.467	0.223	6.30	17.514	19.981	6.30
F	23 36 04.33	12 52 47.3	−2.557	0.143	2.37	19.724	22.281	2.37

NOTE.—Units of right ascension are hours, minutes, and seconds, and units of declination are degrees, arcminutes, and arcseconds.

[a] Refers to the radius at which the colors were determined.

each field a minimum of 4 times, a list was compiled of all possible nonstellar objects in each field that had a minimum diameter of roughly 5 pixels (0″.5 for the WF cameras and 0″.23 for the PC). Automated galaxy search techniques were not employed for this image, as one (FOCAS) had been used on other WFPC2 images and shown to be less reliable than the by-eye search technique (O'Neil, Bothun, & Impey 1998). All objects on the list then had their appearance checked against their image in one of the uncombined frames to ensure that no errors had occurred during the image-processing phase (e.g., image registration errors). Remaining objects were considered potential galaxies and left on the list. It should be noted that because of the low sensitivity in the 300 frames, all galaxy identification was done in the 814 frames. Most of the galaxies were not visible in the 300 frames.

The zero points for each field were taken from the PHOTFLAM value given in the image headers. The zero points from the STMAG system (the Space Telescope system, based on a spectrum with constant flux per unit wavelength set to approximate the Johnson system at V) is

$$\mathrm{ZP_{STMAG}} = -2.5 \log \mathrm{PHOTFLAM} - 21.1 .$$

For the 814 filter, the resultant zero point was 22.93, while for the 300 image the zero points were 19.43 (for the PC image) and 19.46 (for the WF images). Conversion of the zero points for the Vega system was done by comparing the STMAG values of various objects within the field with the known values in both U and I found from the Michigan-Dartmouth-MIT (MDM) 1.3 m telescope images taken of UGC 12695 (see McGaugh 1992 for details on the ground-based images). The determined conversion factors were then $I - 814 = -1.44 \pm 0.05$ and $U - 300 = 0.04 \pm 0.05$. It should be noted that this conversion is from the STMAG system to the Johnson-Cousins bands, not from the "Vega" system used by Holtzman et al. (1995) and others. The dif-

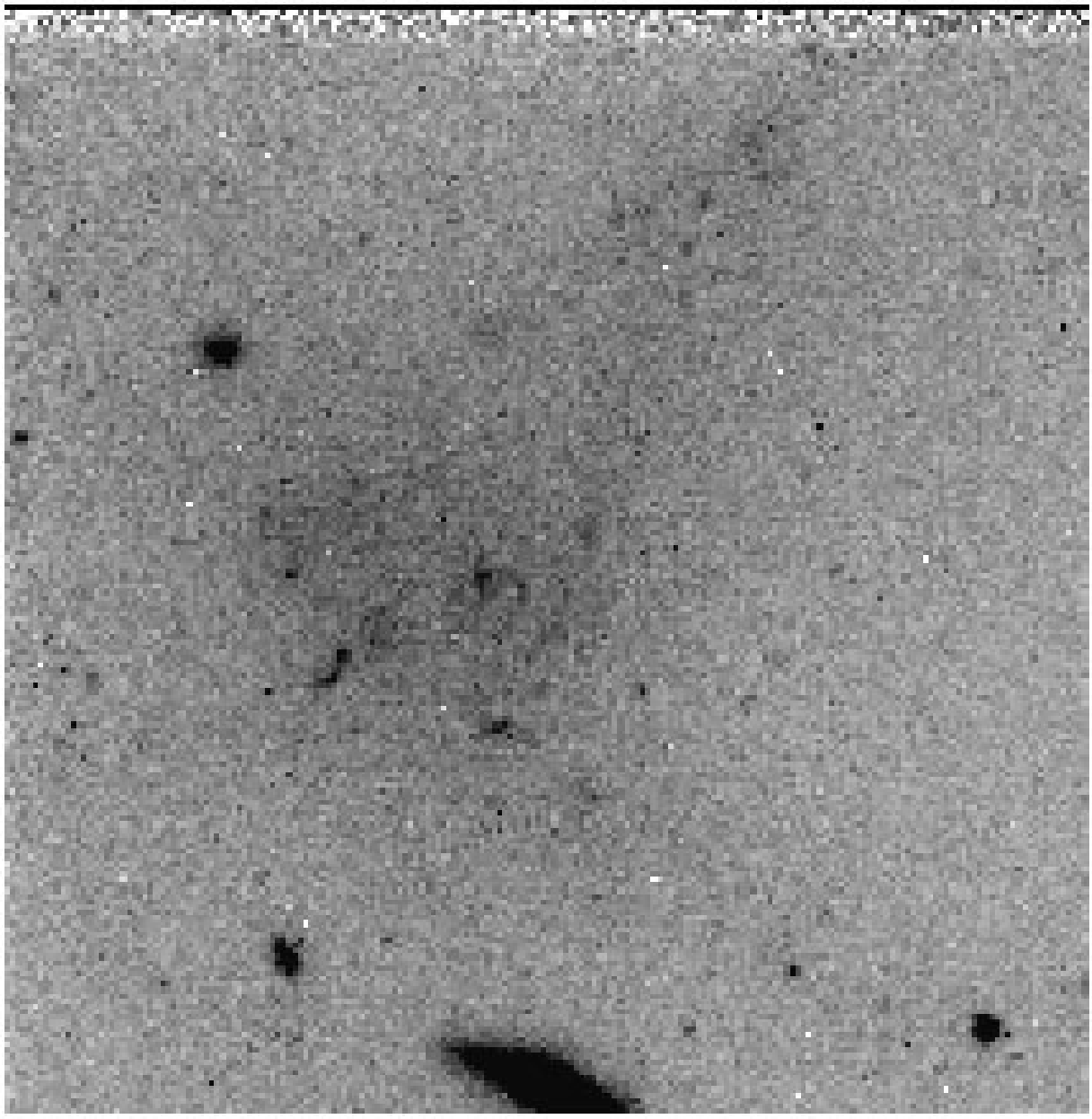

FIG. 4.—Expanded view of the nucleus of UGC 12695 through the WFPC2 814 filter. The image is 20″ × 20″ with the same orientation as Fig. 1*a*.

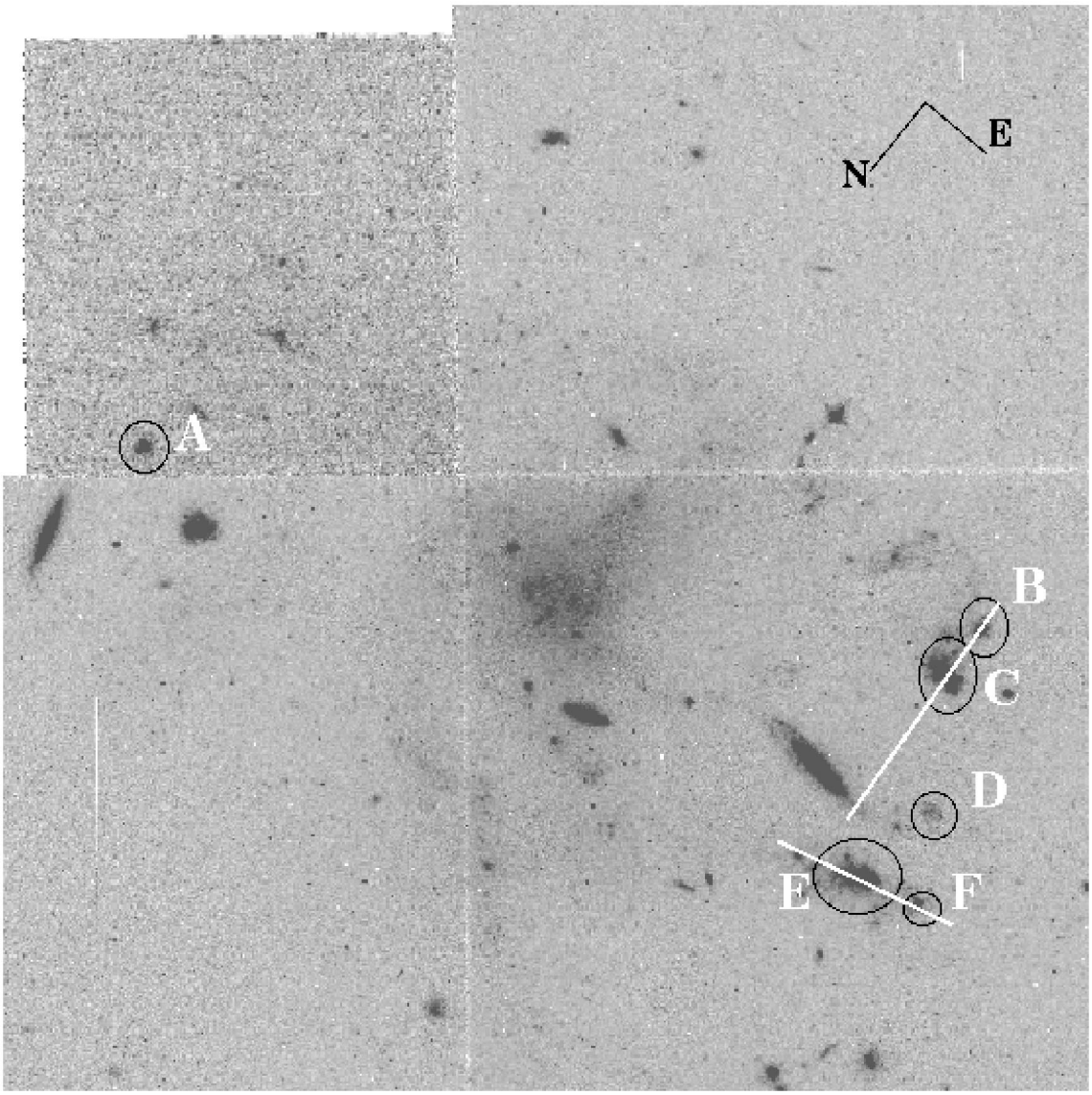

FIG. 5.—Image showing the regions of Hα emission discussed in § 4. The circled regions correspond to the Hα regions listed in Table 3, while the white lines correspond to the spectral slits used by McGaugh (1994) and presented in Table 4.

ference in zero-point conversions to Johnson-Cousins *I* band between these two magnitude systems is substantial for objects with the colors of galaxies. The Appendix provides more information and documentation on this zero-point difference.

The peak intensity for each galaxy was found, and ellipses were fitted around that point to obtain the intensity in each annulus using the modified GASP software (Cawson 1983; Bothun et al. 1986). In the amorphous galaxies, like UGC 12695, the physical center, estimated by centroiding with respect to fitted isophotes, was chosen. In the cases of interacting (or overlaid) galaxies, the competing galaxy was masked, allowing for a surface brightness profile to be obtained for each of the involved galaxies when possible. The core of the point-spread function has a radius of 0.″1 for the PC and 0.″2 for the WF cameras, and the surface brightness profiles cannot be trusted below that. The average sky-subtracted intensity within each (annular) ellipse was found and calibrated with the photometric zero point.

Exponential surface brightness profiles were then derived using

$$\Sigma(r) = \Sigma_0 \, e^{-r/\alpha} , \tag{1}$$

where Σ_0 is the central surface brightness of the disk in linear units ($M_\odot$ pc^{-2}) and α is the exponential scale length in arcseconds. This can also be written (the form used for data analysis) as

$$\mu(r) = \mu(0) + (1.086/\alpha)r , \tag{2}$$

where μ_0 is the central surface brightness in mag arcsec^{-2}.

Galaxy inclination was found using the GASP software to determine the major and minor axes at each isophote. The inclination angle is

$$i = \cos^{-1} (r_{\rm minor}/r_{\rm major}) . \tag{3}$$

Because of the asymmetric nature of most of these galaxies, the use of a flattening term (q_0) as part of the inclination

derivation does not seem appropriate. We estimate that i is accurate only to within $\pm 5°$ when determined in this manner.

3. GLOBAL PROPERTIES OF UGC 12695

With a diffuse, Y-shaped nucleus and a faint spiral arm, UGC 12695 has an unusual morphology, which is apparent even from ground-based images. In addition, this imaging has shown what appears to be a number of bright star-forming knots spread throughout the galaxy (Fig. 2). Morphological classification of these images would suggest that UGC 12695 is not a well-defined spiral and would therefore most likely be classified as a type I irregular galaxy, with sporadic locations of star formation. We emphasize, however, that UGC 12695 is considerably more massive than the prototypical examples defined by the LMC and NGC 4449. Furthermore, the *HST* data have shown that appearances are deceiving, as most of these "star-forming knots" are, in fact, background galaxies clearly shining through the main body of UGC 12695. This discovery changes our view of this galaxy considerably.

Table 1 lists the global properties of UGC 12695, found primarily from previous studies. Rows 1 and 2 give the coordinates (right ascension and declination) in the J2000.0 coordinate system found using the WFPC2 image and the STSDAS METRIC task. Row 3 lists the heliocentric radial velocity obtained from the 21 cm observations of Bothun et al. (1985). Row 4 gives our assumed distances based on a Hubble constant of 75 Mpc km^{-1} s^{-1} and a Virgocentric infall velocity of 300 km s^{-1}. Row 5 gives the total H I mass of the galaxy, with $M_{\rm H\,I} = \log (M_{\rm H\,I}/M_\odot)$, and row 6 gives the total dynamical mass of UGC 12695 ($M_{\rm dyn} = \log [M_{\rm dyn}/M_\odot]$). In row 7 is listed the gas mass–to–luminosity ratio, while row 8 provides the gas mass fraction for the galaxy, with $f_g = M_g/(M_g + M_*)$ (values listed in rows 6–8 come from McGaugh 1992.) Row 9 lists the exponential scale length in kiloparsecs (McGaugh & Bothun 1994). In row 10 is listed the galaxy's absolute magnitude (McGaugh 1992). Row 11 lists the galaxy's central surface brightness determined from equation (2) (McGaugh & Bothun 1994). Finally, rows 12–15 give the galaxy's apparent magnitude and total (luminosity weighted) colors, also from McGaugh & Bothun (1994).

An examination of Table 1 shows that UGC 12695 is quite blue and rich in gas, suggesting that it is now undergoing one of its first episodes of star formation. The chance to study this phenomenon at significantly higher resolution motivated the *HST* observations. The first surprising discovery from the WFPC2 image of UGC 12695 was that many of the objects believed from ground-based observations to be stellar knots contained within UGC 12695 are actually background galaxies that are showing *through* both the galaxy's disk and outer nucleus. The significance of this discovery is twofold—first, the number of putative star-forming regions has been greatly reduced, and second, UGC 12695 is a remarkably transparent galaxy even in its nuclear regions. As all prior photometry of UGC 12695 was performed assuming the background galaxies to be part of UGC 12695, we redetermined the galaxy's surface photometry with the galaxies masked (and the masked pixels replaced with the average values of the surrounding pixels).

The results of redetermining UGC 12695's photometry with the background galaxies masked are shown in the first two rows of Table 2. In the first row, we show the colors derived for UGC 12695 from ground-based images with the background galaxies included in the photometry, while the second row shows the colors of UGC 12695 once these galaxies are masked (see Table 6 below to observe which galaxies were masked during this process and which are too far from the nucleus of UGC 12695 to have been included in any of the photometric calculations). The significance of masking the background galaxies is immediately apparent—masking the background galaxies (which are primarily red; see below) has made this already very blue galaxy significantly bluer. In fact, the resultant $U-I$ color of about -0.2 may make UGC 12695 the bluest known galaxy. It is remarkable that this blue color is achieved without many obvious large-scale regions of star formation being present. It is thus the smooth, diffuse light of this galaxy, coupled with small-scale regions of star formation, that is very blue. This assertion is documented below.

Taking advantage of the high resolution of the WFPC2 images, we further explored UGC 12695's global properties by masking the six Hα star-forming regions listed in Table 3 and determined from ground-based images taken at the MDM 1.3 m McGraw-Hill Telescope. The third row of Table 2 shows the colors of UGC 12695 with both the known background galaxies and the Hα regions removed. Significantly, no measurable difference between the second and third rows can be noted. In addition, Figure 3 shows the (814 band) surface brightness profile of UGC 12695 with all background galaxies and Hα regions included in the analysis (*solid line*), UGC 12695 with all the definite background galaxies removed (*dashed line*), and UGC 12695 with both the background galaxies and all the Hα regions removed (*dash-dotted line*). No differences are apparent in the plots until after $r = 20''$, and no difference in the overall profile of the galaxy can be seen at any radius.

The discovery of background galaxies shining through UGC 12695 dramatically impacts the galaxy's nuclear (inner 10″) color. It should be noted, though, that as these

TABLE 4

METALLICITY OF SELECT Hα REGIONS IN UGC 12695

Region	log (O/H)	log (N/H)	log (Ne/H)
s1a1.....	−4.18	−6.52	−4.84
s1a2.....	−3.98	−5.66	−4.76
s1a3.....	−4.01	−5.81	−4.86
s2a1.....	−4.08	−5.81	−4.83
s2a2.....	−4.09	−5.62	−4.96
s2a3.....	−3.92	...	−4.95

NOTE.—From McGaugh 1994.

TABLE 5

PHOTOMETRY OF SELECT REGIONS WITHIN Hα AREAS B AND C

Region	Color
1	300−814 = −2.499
2	300−814 = −2.481
3	300−814 = −2.950
4	300−814 = −2.555
5	300−814 = −2.633
6	300−814 = −5.076
7	300−814 = −2.537
8	300−814 = −1.820
Inner 2″ (nucleus)	814−300 = −0.541
Inner 10″ (nucleus).....	814−300 = −0.977

TABLE 6

PHOTOMETRIC AND STRUCTURAL PARAMETERS DERIVED FOR THE BACKGROUND GALAXIES

Name (1)	R.A. (J2000.0) (2)	Decl. (J2000.0) (3)	300−814 (4)	$U-I$ (5)	300_T (6)	814_T (7)	$814_T(\alpha)$ (8)	α (arcsec) (9)	μ_0 (10)	$\mu_{0,c}$ (11)	R_T (arcsec) (12)	i (13)
U2-8	23 36 01.64	12 53 27.3	>-1.02	>1.68	>22.56	23.581	23.090	0.380	22.987	23.487	0.894	50.9
U2-14.....	23 35 58.22	12 52 59.7	>-1.38	>1.32	>21.18	22.561	22.986	0.246	21.932	22.263	1.415	42.5
U2-17.....	23 36 02.66	12 53 34.3	>-0.33	>2.37	>21.18	21.511	21.212	0.632	22.209	22.719	1.823	51.3
U2-18.....	23 35 58.48	12 53 49.9	>1.62	>4.32	>21.18	19.561	18.164	1.033	20.223	20.755	4.127	52.0
U2-20[a].....	23 36 02.06	12 53 06.4	>-1.40	>1.31	>21.18	22.571	22.165	0.539	22.817	22.878	1.207	19.1
U2-22[a].....	23 36 00.07	12 52 36.2	-0.867	1.833	20.864	20.991	20.317	0.800	21.828	21.891	1.884	19.3
U2-23[a].....	23 35 59.33	12 52 40.1	-0.517	2.183	21.444	20.461	18.694	1.362	21.360	22.560	4.277	70.7
U2-24.....	23 35 58.13	12 53 56.5	>-2.89	>-0.19	>21.18	24.071	23.70	0.297	23.058	23.911	0.586	62.9
U2-36[a].....	23 36 04.35	12 52 59.9	>-0.95	>1.75	>21.19	22.141	21.220	0.537	21.864	22.185	1.270	41.9
U2-39[a].....	23 36 03.58	12 52 39.1	>1.28	>3.98	>21.19	19.911	18.475	1.314	21.063	22.465	5.596	74.0
U2-41.....	23 36 03.94	12 53 04.1	>0.92	>3.62	>21.19	20.271	20.301	0.086	16.969	17.564	1.512	54.5
U2-45[a].....	23 36 02.36	12 52 41.0	>0.70	>3.40	>21.19	20.491	19.437	0.863	21.111	21.971	0.863	63.1
U2-46[b].....	23 36 06.68	12 52 27.1	...	...	...	...	...	...	...	...	...	...
U2-48.....	23 36 07.16	12 53 04.7	>-1.23	>1.47	>21.19	22.421	22.634	0.367	22.515	22.845	0.367	42.4
U2-53[b].....	23 36 03.07	12 53 37.1	...	...	...	...	...	...	...	...	...	...
U2-65.....	23 36 01.84	12 51 53.4	>-3.30	>-0.59	>21.12	24.411	24.173	0.199	23.448	22.667	0.199	60.9
U2-67.....	23 36 04.74	12 51 59.4	>-1.96	>0.74	>21.12	23.081	22.971	0.408	23.022	23.830	0.948	61.6
U2-68.....	23 36 04.27	12 51 04.1	>-0.34	>2.36	>21.12	21.461	21.405	0.363	21.099	21.654	2.219	53.1
U2-70.....	23 36 04.21	12 51 19.7	>-1.66	>1.04	>21.12	22.781	22.841	0.206	21.400	21.593	1.109	33.2
U2-72.....	23 36 01.22	12 51 59.1	>-1.21	>1.49	>21.12	22.331	21.150	0.726	22.449	22.927	1.394	29.9
U2-74.....	23 36 02.09	12 52 20.2	>0.36	>3.06	>21.12	20.761	21.283	0.454	21.565	22.290	2.050	59.1

[a] Masked while determining the photometry of UGC 12695 (Table 2, rows 2 and 3). Other than U2-74, the other galaxies in this table are located too far from the nucleus of UGC 12695 to have been included in any of the WFPC2 photometry. U2-74 was not masked, as its identity as a background galaxy is unsure.

[b] Galaxy is on the edge of the WFPC2 image. Photometry was not possible.

galaxies appear primarily through the 814 (I band) filter, and mostly "dropped out" when viewed through either the (ground-based) B band or the 300 images, the removal of the galaxies does not affect, among others, the overall magnitude, surface brightness, and gas fraction of UGC 12695 listed in Table 1 and found using the blue luminosity. Hence, the primary effect of the mistaken inclusion of these background galaxies in prior studies is in the total I-band luminosity and the derived $U-I$ or $V-I$ colors. Removal of these galaxies significantly lowers these values.

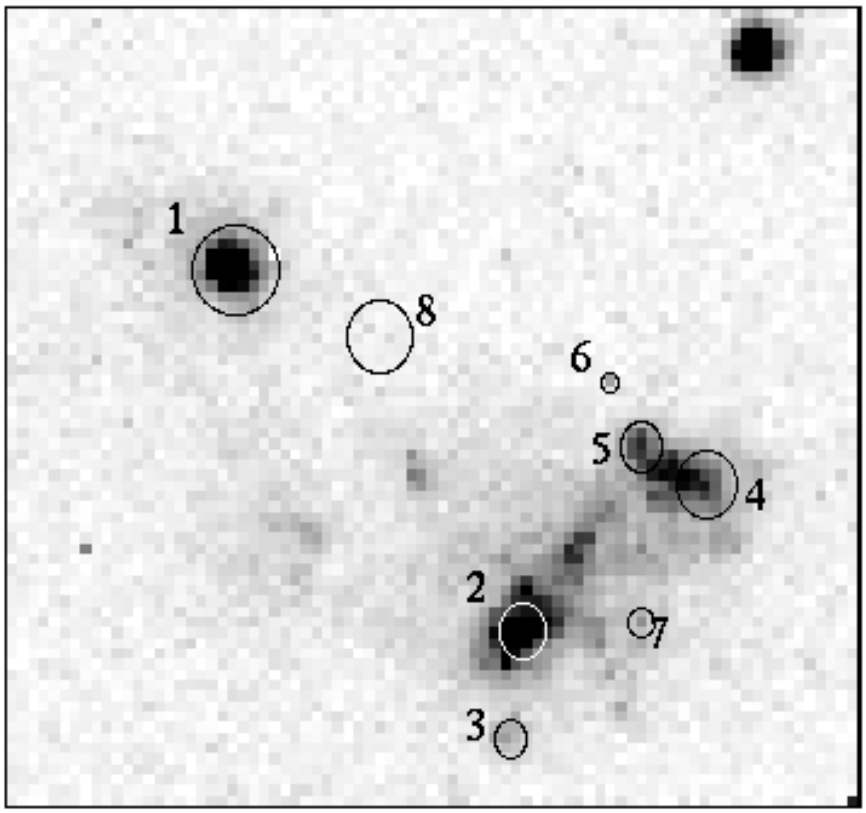

FIG. 6.—Images of Hα areas B and C, discussed in § 4. The image is 1″ across. This image is the inverse (across the vertical axis) of Fig. 5.

4. STAR FORMATION IN UGC 12695

The high resolution of the *HST* WFPC2 cameras allows for an unprecedented view of the stellar structure of UGC 12695. Examining the 814 image of UGC 12695 (Fig. 1*a*) shows a number of distinct star-forming regions surrounding a fairly diffuse, irregular nucleus. In addition, a spiral arm can be seen encircling the nucleus, which consists of disjointed stellar knots. Figure 4 shows a gray-scale image of the inner 10″ of UGC 12695. Highly noncircular in appearance, the nucleus of UGC 12695 consists of distinct regions of star formation clustered primarily in the northern (*bottom*) portion. Other than these localized regions of star formation, even the nuclear regions of UGC 12695 are transparent to the point that a spiral background galaxy can be identified clearly (Fig. 4, *bottom edge*). We do note, however, that this nuclear region is significantly redder than the galaxy as a whole (see Table 2) and thus likely contains the bulk of any old stellar population that might be present. The LSB nature of this galaxy, however, strongly indicates that this older population is distributed in a very diffuse manner and is certainly not concentrated into a central bulge or bar.

A number of regions of Hα emission are also present within UGC 12695, many of which are visible in the ground-based images (Fig. 2*e*). Photometry of these areas is given in Table 3, with the detailed areas studied shown in Figure 5. The majority of these areas are fairly small, with $r_{27} \lesssim 2\farcs6$ (0.8 kpc) (the only exception is area E, which has a radius of 6″.4 [2 kpc]). The colors of these regions are extremely blue, with $0.1 \lesssim U-I \lesssim 0.5$, indicating a significant level of current star formation.

McGaugh (1992) performed a metallicity study on a number of Hα regions in UGC 12695. The slit positions used are shown as white lines in Figure 5, while the results from that work are given in Table 4. Slit one (s1) runs east-west through the northern Hα areas, while slit two (s2) runs roughly north-south through the southern areas. The area labeled s2a3 (unfortunately) lies on an Hα area that is overshadowed in the 814 image by a bright background galaxy. The metallicities of these areas are low, around 0.4 $Z_{\odot}$. Combined with the extremely blue colors of the regions of Hα regions, this indicates that these regions are likely young starburst areas that have not yet enriched much of the gas.

A further look at two of these regions of Hα emission (areas B and C) is given in Figure 6. We have determined the $814-300$ colors of localized regions within these Hα areas, with the results listed in Table 5. Regions 1–8 within

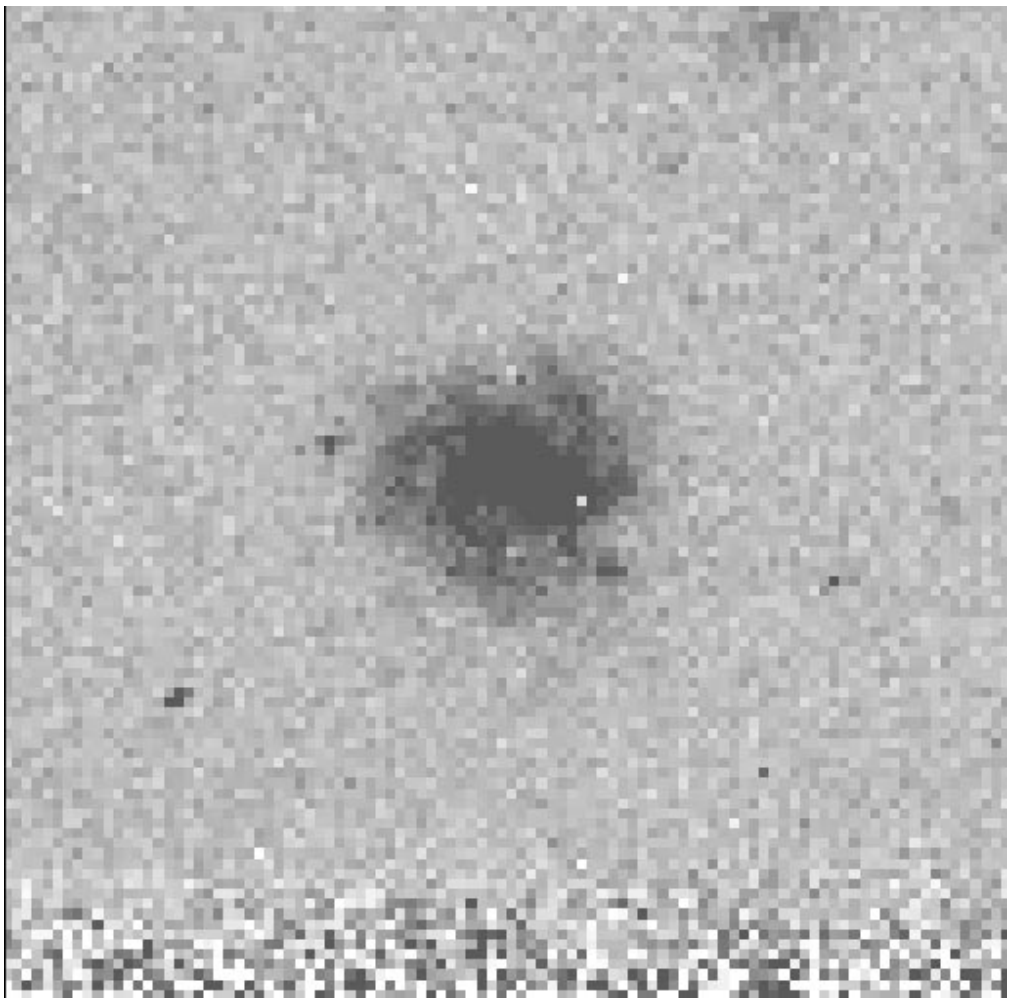

FIG. 7*a*

FIG. 7.—Images of the four largest background galaxies through the 814 filter. The images are of (*a*) U2-22, (*b*) U2-23, (*c*) U2-39, and (*d*) U2-45.

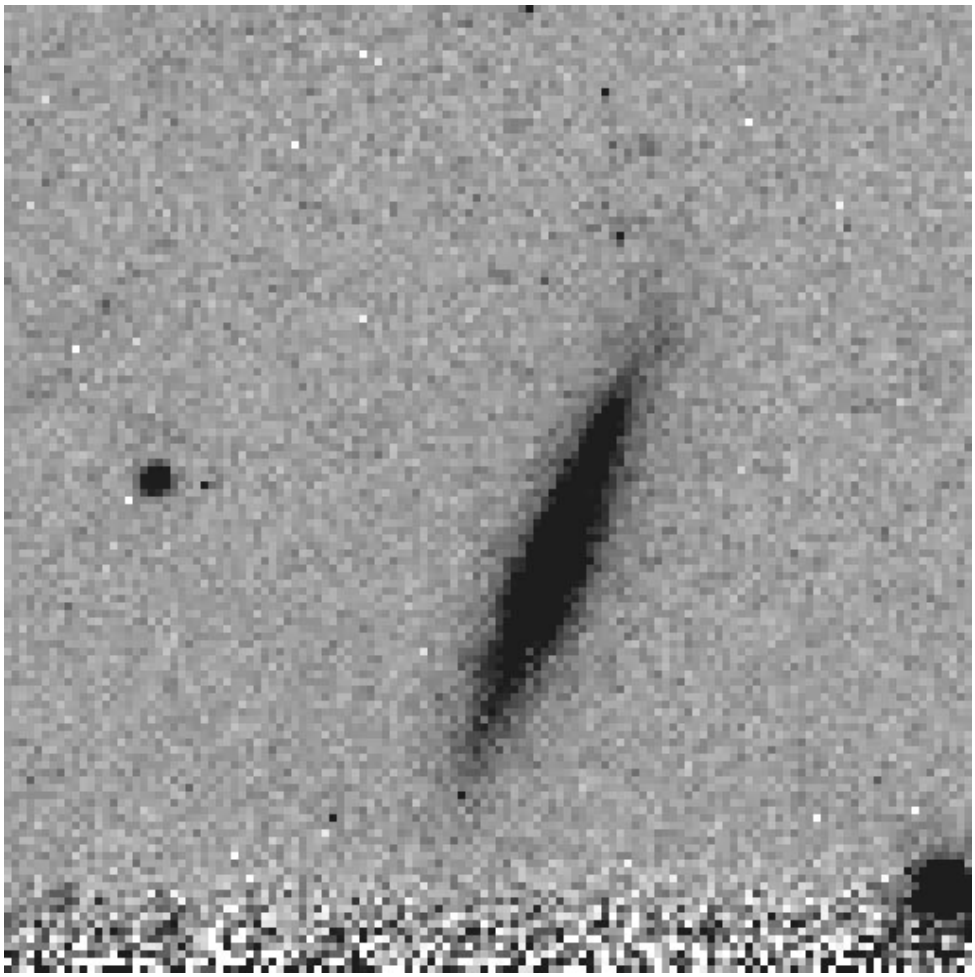

FIG. 7*b*

the Hα area were chosen to encompass various regions of localized starburst. The colors of these regions are exceptionally blue, and thus they are likely comprised primarily of young stellar types. Significantly, though, region 8, which, although clearly associated with the Hα areas, does not encompass a region of apparent significant star-forming activity, also has an 814−300 color that is at least 1 mag bluer than the nuclear region of UGC 12695. It is thus clear that the majority of the current star formation in UGC 12695 is happening within very localized (small spatial scale), noncentralized, star-forming regions that are dispersed throughout the galaxy.

TABLE 7

COLORS OF EIGHT OF THE BACKGROUND GALAXIES IDENTIFIED IN THE GROUND-BASED (MDM) IMAGES

Name	$B-V$	$V-I$	Radius (arcsec)
U2-17	...	>1.92	1.82
U2-22	>0.88	1.40	1.10
U2-23	>0.00	1.91	0.95
U2-36	...	>1.29	1.27
U2-39	$\gtrsim -0.12$[a]	0.16	5.50
U2-41	>0.49	3.07	1.55
U2-45	[a]	1.75	0.86
U2-72	> −1.34	2.84	1.40

[a] Lies behind the nucleus of UGC 12695.

5. BACKGROUND GALAXIES

As these are short-exposure images of the nuclear region of a nearby galaxy, the existence of any background galaxies in our image was a great surprise. The fact that we discovered 21 potential background galaxies is proof of the fairly transparent nature of UGC 12695, as well as the excellent ability of *HST* WFPC observations to detect distant galaxies no matter where it is pointed.

Details of the galaxy identification and analysis techniques are given in § 2 above, while the results, as applied to these background galaxies, are listed in Table 6 and described below. The 814-band detection limit was 24.5 mag.

Column (*1*).—The name given to each of these galaxies (none have been previously identified). The numbering system is based on all objects identified in the image, including foreground stars, image flaws, and regions of Hα emission.

Columns (*2*) *and* (*3*).—Right ascension and declination in J2000.0 coordinates, determined using the STSDAS METRIC task.

Column (*4*).—The 814−300 color of the galaxies. If the galaxy could not be identified in the 300 image, a maximum apparent brightness (magnitude) was determined by assuming the galaxy would have been identified if its radius exceeded 5 pixels and it had an average brightness greater

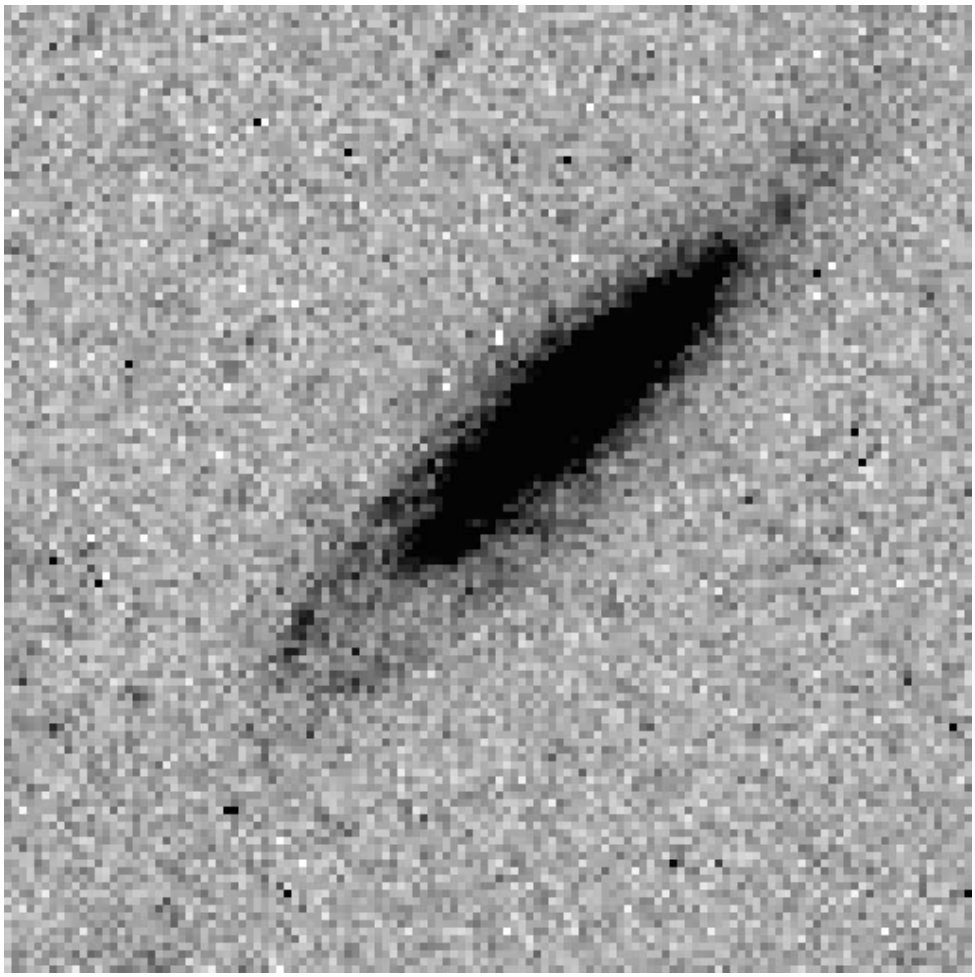

FIG. 7*c*

than 3 σ above the sky (sky brightness was determined separately for each of the four WFPC2 frames).

Column (*5*).—The $U-I$ color of each galaxy as described in § 2.

Columns (*6*) *and* (*7*).—The total magnitude of the galaxy through both the 814 and 300 filters. Magnitudes are corrected for Galactic extinction (treating the 814 filter as a Johnson *I*-band filter and the 300 filter as a Johnson *U*-band filter), but not for inclination or redshift (*k*-correction).

Column (*8*).—The total integrated magnitude of the galaxy through the 814 band, using

$$\text{mag}\ (\alpha) = \mu(0) - 2.5 \log 2\pi\alpha^2\ , \qquad (4)$$

where α is the exponential scale length in arcseconds. If an exponential profile was not fitted to a particular galaxy's surface brightness profile, no value is listed in this column. It should be noted that on occasion (e.g., U2-18), the magnitude in this column is considerably brighter than that given in column (7). In these cases, the maximum aperture size used in calculating the total magnitude (col. [7]) was smaller than the actual galaxy size, typically as a result of interference from a neighboring galaxy or from UGC 12695. The integrated magnitude given in this column is thus the more accurate one.

Column (*9*).—The exponential scale length of the galaxy found using equation (2).

Column (*10*).—The central surface brightness of the galaxy in mag arcsec^{-2} as defined in equation (2). When a surface brightness profile was found for a galaxy yet no line was fitted to it, the central surface brightness was estimated.

Column (*11*).—The inclination-corrected central surface brightness in mag arcsec^{-2},

$$\mu_e(0) = \mu(0) - 2.5 \log \cos i\ , \qquad (5)$$

where the inclination used is listed in column (13). Note that this is a geometric path-length correction that assumes no dust and, therefore, may not be accurate for these galaxies.

Column (*12*).—The major-axis radius in arcseconds as measured at the $\mu_{814} = 25.0$ mag arcsec^{-2} isophote. If the surface brightness profile errors exceeded 0.25 mag arcsec^{-2} before $\mu_{814} = 25.0$ mag arcsec^{-2}, then the largest accurate radius is given.

Column (*13*).—The inclination angle (in degrees) as found by the GASP software (eq. [3]). The angle is correct to within $\pm 5°$ (the error is primarily due to the galaxies' lack of azimuthal symmetry).

Eight of the galaxies were large and bright enough to be identified within the MDM images. These galaxies are listed in Table 7, along with their colors as determined from the ground-based images. As these are distant galaxies, none could be reliably identified through the *B*-band image, and a few could not even be identified in the *V*-band image. In

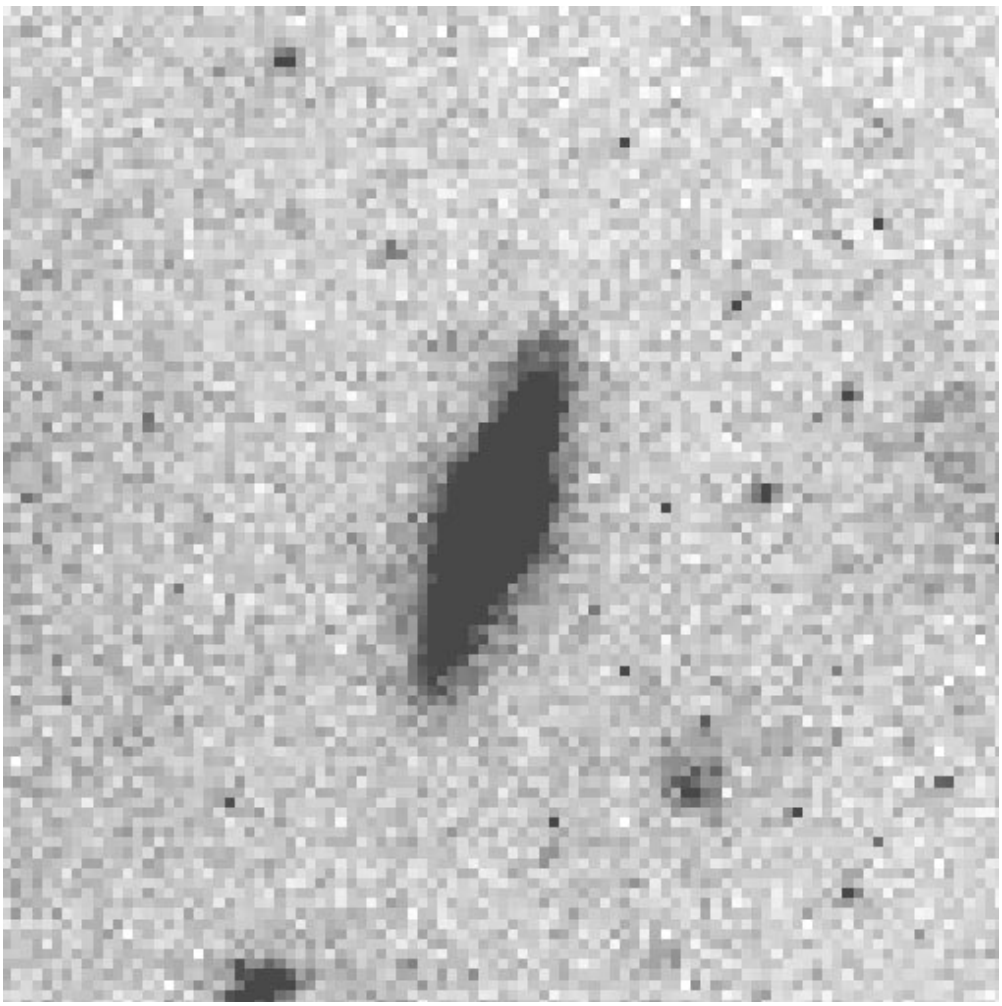

FIG. 7*d*

these cases, the maximum apparent magnitude was determined for the "dropout" band as described above, using a minimum detection radius of 3 pixels.

The majority of the galaxies discovered have sizes $\lesssim 1''.5$, making a morphological description difficult at best. A few of the galaxies, though, are fairly large and thus could be examined more closely. Figure 7 shows the four largest background galaxies discovered in our image. All four appear to be well-formed spiral galaxies with little of the irregular morphology evident in deeper *HST* WFPC2 surveys, such as the Hubble Deep Field (Williams et al. 1996). Follow-up spectroscopy of these galaxies is clearly desirable.

Comparing the values of these background galaxies with the colors, sizes, and magnitudes of both the medium and deep *HST* surveys leads to the conclusion that the background galaxies in our survey lie at a redshift of $0.5 \lesssim z \lesssim 1.5$. The radii of the galaxies in the Medium Deep Survey (MDS) lie between $1''.2$ and $2''.2$, while the $V-I$ color of the MDS galaxies is $0.1 \lesssim V-I \lesssim 3.0$, with $\langle V-I \rangle = 1.2$ and the survey ranging over $20.0 \lesssim m_{814} \lesssim 22.0$. The background galaxies in our survey thus lie at the red edge of this color spectrum and are typically smaller (in apparent size) than those in the MDS. As the MDS galaxies were determined to lie in the range $0.5 \lesssim z \lesssim 1.0$, we conclude the background galaxies in our survey lie at least that distant, or at $0.5 \lesssim z \lesssim 1.5$. In order to more fully understand the morphology and distribution of these galaxies, and to thereby gain a firmer understanding of galaxy morphological evolution, a more detailed look at these galaxies through multiple filters and at longer exposure times is definitely warranted.

6. DISCUSSION AND CONCLUSION

UGC 12695 is a remarkable galaxy. It has an exceptionally high gas mass fraction, very low metallicity, a strikingly diffuse morphology with perhaps the bluest colors known for a galaxy, and an exceedingly transparent nature. Combined, these attributes indicate that UGC 12695 is a highly unevolved galaxy. Since UGC 12695 is at rather low redshift ($z \sim 0.021$), its properties indicate that some potentials may well have late collapse and formation timescales (such as may also be the case in NGC 1705, another apparently young galaxy; see Meurer et al. 1992). The discovery of apparently young galaxies at low redshift has considerable importance for understanding galaxy evolution. As it is unlikely there is anything unique about UGC 12695, one would reasonably expect objects like it to exist at any redshift. However, the LSB nature of UGC 12695 makes it difficult to detect. Indeed, it seems ironic that an apparently

unevolved galaxy would itself be difficult to detect because of its low surface brightness. This obviously has important implications for detecting young galaxies at any redshift.

Understanding the evolution of UGC 12695 might shed considerable light on galaxy formation scenarios as a whole. Unlike most galaxies, UGC 12695 also has the advantage of being relatively isolated, with its nearest neighbor located at a projected distance of $\sim$200 kpc. UGC 12695 is likely to have been influenced minimally (if at all) by other galaxies. Clues to the formation of UGC 12695 may be found in its structural peculiarities. The galaxy's low overall density is manifest in its dynamical ratio of mass to total size, as well as its transparent nature. The inferred low mass density of UGC 12695 (and LSB disks in general; see de Blok & McGaugh 1997) may mean that stellar orbits are not well defined in this potential, thus resulting in the observed non-circular nature of even the inner nucleus and the fact that the majority of the star formation is taking place in non-centralized, yet strongly localized regions spread throughout the diffuse galaxy body. Whatever is the case, the overall properties indicate that UGC 12695 is still highly unevolved. The clear fact that this object has escaped our attention, as a result of its diffuse nature, causes concern over how many other examples of this phenomenon in the nearby universe have been missed to date.

This research has made use of the NASA/IPAC Extragalactic Database, which is operated by the Jet Propulsion Laboratory, California Institute of Technology, under contract with the National Aeronautics and Space Administration.

APPENDIX

PHOTOMETRIC CALIBRATION OF *HST* WFPC2 IMAGES

The calibration we have used in converting our 814 data to the Johnson-Cousins system is substantially different from the values given in Holtzmann et al. (1995). The primary reason for this is that our instrumental zero point is based on the Space Telescope (ST) magnitude system, while the Holtzmann et al. values use Vega to define the zero point. As detailed by Whitmore in the WFPC2 photometry manual (STScI internal publication; see also Whitmore 1995), the difference in conversion factors is substantial. This is because the 814 filter is a close approximation to Johnson-Cousins I, but the definition of ST magnitudes for a star of color corresponding to K0 III (a reasonable approximation to the spectral energy distribution of a galaxy) is different by 1.2 mag than if Vega were used as the zero point. Since this difference may not be widely known in the community, unless the WFPC2 photometry documentation has been read carefully (specifically, chapter 41), we give a brief synopsis here.

Both the 300 and 814 filters are wide-bandpass filters designed to maximize throughput and were not designed to specifically match a standard filter bandpass. The STMAG system exists with the true filter design in mind and is based on a spectrum with constant flux per unit wavelength. Conversion from data numbers DN to the STMAG system is thus straightforward:

$$\mathrm{STMAG} = -2.5 \log (\mathrm{DN/exposure\ time}) - 2.5 \log \mathrm{PHOTFLAM} - 21.1 ,$$

where PHOTFLAM is a value obtained by STScI using standard-star calibrations with the four WFPC2 chips and takes into account, among other things, distortions and plate scale. Because the STMAG system is not a standard magnitude system, though, conversion from the DN is often instead done to a more conventional system based on Vega's spectrum (e.g., Holtzmann et al. 1995; Driver, Windhorst, & Griffiths 1995). Conversion from the STMAG system to the Vega system is typically done through $814_{\mathrm{STMAG}} - 814_{\mathrm{Vega}} \approx -1.226$, $300_{\mathrm{STMAG}} - 300_{\mathrm{Vega}} \approx -0.05$. Whichever of these systems is chosen, though, additional corrections need to be made to convert the data to Johnson-Cousins colors.

Before discussing the additional corrections necessary for conversion to the Johnson-Cousins system, an additional factor needs to be considered. WFPC2 images can be taken with two different gain settings, 7 and 14 e^- ADU^{-1}. The calculations done by Holtzman et al. (1995) are for the gain = 14 setup, while the data contained in this paper, as well as the majority of recent WFPC2 data, were taken with the gain setting of 7. This results in a difference of roughly $-2.5 \log 2 \approx -0.75$ but, of course, has a further dependence on the spectral energy distribution of the source.

Our ground-based I-band data, which are used to convert the 814 data to the Johnson-Cousins system, were obtained through the standard KPNO filter set. This I-band filter has $\lambda_{\mathrm{peak}} = 8290 \pm 40$ Å and $\Delta\lambda(\mathrm{FWHM}) = 1950$ Å. The traditional Johnson I-band filter has λ_{peak} 9000 Å and $\Delta\lambda(\mathrm{FWHM}) = 2400$ Å. Because CCDs have considerably more red sensitivity than the old S-20 phototube, the peak wavelength of the I-band filter used for CCD observations is significantly bluer. The 814 filter used in the *HST* observations has $\lambda_{\mathrm{peak}} = 8386$ Å, $\langle\lambda\rangle = 8269$ Å, and $\Delta\lambda(\mathrm{FWHM}) = 1758$ Å, values that are similar to the I-band filter used from the ground. Had both the ground-based and *HST* data been calibrated against Vega, we would have recovered the Holtzmann et al. (1995) conversion. The much larger conversion that we found (i.e., 1.4 mag) is due almost entirely to the use of the STMAG system for our WFPC2 data with a gain setting of 7 instead of 14 (again, this is all discussed in chapter 41 of the WFPC2 photometry manual).

REFERENCES

Bothun, G. D., Beers, T. C., Mould, J. R., & Huchra, J. P. 1985, AJ, 90, 2487
Bothun, G., Impey, C., & McGaugh, S. 1997, PASP, 109, 745
Bothun, G. D., Mould, J. R., Caldwell, N., & MacGillivray, H. T. 1986, AJ, 92, 1007
Bottinelli, L., Gouguenheim, L., Fouqué, P., & Paturel, G. 1990, A&AS, 82, 391
Cawson, M. 1983, Ph.D. thesis, Univ. Cambridge
de Blok, W. J. G., & McGaugh, S. 1997, MNRAS, 290, 533
Driver, S. P., Windhorst, R. A., & Griffiths, R. E. 1995, ApJ, 453, 48
Holtzman, J. A., Burrows, C. J., Casertano, S., Hester, J. J., Trauger, J. T., Watson, A. M., & Worthey, G. 1995, PASP, 107, 1065
Klein, U., Giovanardi, C., Altschuler, D. R., & Wunderlich, E. 1992, A&A, 255, 49
Lewis, B. M. 1987, ApJS, 63, 515

McGaugh, S. S. 1992, Ph.D. thesis, Univ. Michigan Ann Arbor
McGaugh, S. S. 1994, ApJ, 426, 135
McGaugh, S. S., & Bothun, G. D. 1994, AJ, 107, 530
McGaugh, S. S., & de Blok, W. J. G. 1997, ApJ, 481, 689
McGaugh, S. S., Schombert, J. M., & Bothun, G. D. 1995, AJ, 109, 2019
Meurer, G. R., Freeman, K. C., Dopita, M. A., & Cacciari, C. 1992, AJ, 103, 60
O'Neil, K., Bothun, G. D., & Impey, C. D. 1998, in preparation
O'Neil, K., Bothun, G. D., Schombert, J., Cornell, M. E., & Impey, C. D. 1997, AJ, 114, 2448
Schneider, S. E., Thuan, T. X., Magri, C., & Wadiak, J. E. 1990, ApJS, 72, 245
Whitmore, B. 1995, in Calibrating *Hubble Space Telescope*: Post Servicing Mission, ed. A. Koratkar & C. Leitherer (Baltimore: STScI), 269
Williams, R. E., et al. 1996, AJ, 112, 1335